

Microstructural control of polymers achieved using controlled phase separation during 3D printing with oligomer libraries: dictating drug release for personalized subdermal implants

Laura Ruiz-Cantu, Gustavo F. Trindade, Vincenzo Taresco, Zuoxin Zhou, Laurence Burroughs, Elizabeth A. Clark, Felicity R.A.J. Rose, Morgan Alexander, Christopher Tuck, Richard Hague, Clive Roberts, Derek J. Irvine, Ricky D. Wildman**

Dr. L. Ruiz-Cantu, Dr. Z. Zhou, Prof. C. Tuck, Prof. R. Hague, Prof. D. Irvine, Prof. R. Wildman

Centre for Additive Manufacturing, Faculty of Engineering, University of Nottingham, Nottingham, NG7 2RD, UK

E-mail: Derek.Irvine@nottingham.ac.uk, Ricky.Wildman@nottingham.ac.uk

Dr. G. F. Trindade, Dr. L. Burroughs, Dr E. A. Clark, Prof. M. Alexander, Prof. C. Roberts
Advanced Materials and Healthcare Technologies Division, School of Pharmacy
University of Nottingham
Nottingham, NG7 2RD, UK

Dr. V. Taresco
School of Chemistry, University of Nottingham
Nottingham, NG7 2RD, UK

Prof. F. Rose
Biodiscovery Institute, School of Pharmacy, University of Nottingham
Nottingham, NG7 2RD, UK

Keywords: 3D printing, drug release, microstructure, biodegradable polymers, phase separation.

Controlling the microstructure of materials by means of phase separation is a versatile tool for optimizing material properties. In this study, we show that ink jet 3D printing of polymer blends gives rise to controllable phase separation that can be used to tailor the release of drugs. We predicted phase separation using high throughput screening combined with a model based on the Flory-Huggins interaction parameter, and were able to show that drug release from 3D printed structures can be predicted from observations based on single drops of mixtures. This new understanding gives us hierarchical compositional control, from droplet to device, allowing release to be ‘dialed up’ without any manipulation of geometry. This is an important advance for implants that need to be delivered by cannula, where the shape is

highly constrained and thus the usual geometrical freedoms associated with 3D printing cannot be exploited, bringing a hitherto unseen level of understanding to emergent material properties of 3D printing.

Often it is not possible to exploit design freedoms due to limitations in the manufacture or the implementation of a device. A pertinent example is the long-term subdermal delivery implant. This is usually cylindrical with a size (maximum diameter 2 mm, length range 1 to 4 cm) defined by a combination of implantation method and anatomical positioning^[1-3]. Currently, such devices are manufactured by a process which heats a blend of polymer and active pharmaceutical ingredient (API) to around 100°C, extrudes and then cuts them to size.^[4,5] However, current systems are not personalizable, nor is it possible to combine multiple drugs into a single treatment. One route to achieving personalization is through 3D printing. Recent advances in 3D printing have shown it can be used for controlling drug elution, most commonly through variation in geometry, or variation in composition^[6,7]. Whilst Fused Deposition Modelling and Binder Jetting are popular and show promise, for the manufacture of implants they are limited by their resolution. Ink jet based 3D printing, however, offers multiple benefits including its scalability, high resolution and importantly, drop by drop deposition that can provide both control over material properties at the microscale as well as the ability to co-deposit multiple materials (drugs). In this work, we exploit the latter to develop microstructural control at the sub droplet level which then permits the precise tailoring of the drug release. This microstructuring only emerges as a function of the drop by drop deposition inherent to ink jet printing.

In developing this concept, we report the creation of a library of multicomponent inks, whose diversity of physicochemical properties allows for the range of phase separation behaviour required for tailoring drug release. We show that, by understanding the

mechanisms that drive formation of this microstructure, we can predict microstructure that arises out of the ink jet printing process and reliably design and manufacture implants for tailored release.

Materials Library

To create the library of printable, functional materials, we first synthesized a range of low molecular weight (5 kDa) biodegradable oligomers with the following head-terminal group combinations, -OH, MA-OH and MA-A (**Figure S2**). The end functionalities were varied to control; (a) the drug release by influencing chain-end centered degradation, and (b) reactivity. The oligomers (PCL, PLA and PTMC) were synthesized from three core monomers (ϵ -caprolactone, DL-lactic acid and trimethylene carbonate), offering a range of degradation rate/mode, crystallinity and thermal/mechanical properties. These polymers are widespread in the biomedical industry, and selected for an easier pathway to adoption compared to completely new materials.^[8] The oligomers were synthesized by ring opening polymerization using metal free organocatalysis,^[9] chosen for low toxicological impact of any subsequent medical devices.^[10]

The library was created by combining nine hydrophobic oligomers in a 1:1 ratio with two relatively hydrophilic reactive solvents, n-vinyl pyrrolidone (NVP) and poly(ethylene glycol diacrylate) (PEGDA) 250 M_w, giving a total of 18 inks (**Figure S3**). After degradation studies, we formulated with a combination of NVP and PEGDA to further tune the degradation behaviour and enhance the structural integrity of the fast release formulations.

Screening materials at the drop scale (10 picolitres)

Microarrays of single drops of each of our 18 inks were rapidly deposited and cured on a glass slide using a high throughput (HTP) method, ready for characterization (see

supplementary).^[11] In this single drop screening (SDS) images were taken of single 200 μm spots (**Figure 1B**), each representing the deposited drops within ink-jet processes. Drops' surface chemical and microstructure/phase separation properties were evaluated using optical microscopy, time-of-flight secondary ion mass spectrometry (ToF SIMS) and automated peak force quantitative nanomechanics (QNM) atomic force microscopy (AFM). This analytical combination provided the phase separation and oligomer distribution data (**Figure 1B and Figure S4**) required to create a phase separation 'taxonomy' which was then related to a Flory-Huggins interaction parameter (χ) prediction of the likelihood of phase separation (see supplementary, **Table S1-2**) (**Figure 1C**). Our observations indicated that the mixtures exhibit three different types of microstructures, (a) homogeneous, completely interspersed mixture (b) dispersed droplets indicating nucleation and growth of domains and (c) spinodal decomposition (core-shell) mixture (**Figure 1B**). Consequently, the materials were ordered according to their χ values and compared to the observed microstructure taxonomy (**Figure 1C**). Broadly, the material microstructure conformed to classification by χ and approximate χ values demarking boundaries between microstructure types were identified: (a) below 0.025 presented one single phase (b) with values between 0.025 and 0.06 phase separated into dispersed droplets and (c) above 0.06 exhibited a core-shell microstructure.

These material combinations were further screened using a HTP methodology designed to assess "printability" to eliminate those materials that cannot be easily printed using ink-jet printing (**Table S3-5**).^[12]

Macro-scale cast samples (15 microliters)

Degradation rate: To determine the influence of microstructure on the cured ink's macro-material/degradation, cast cylinders (length 4 mm, radius 0.5 mm) of the 18 inks were prepared and subjected to degradation studies. The duration of degradation was sixteen weeks

and the mass loss rates are shown in **Figure 2A** and **Figure S5**. As most of the structures printed with NVP didn't maintain their integrity following curing, we replaced the NVP only formulations with PEGDA/NVP solvent combinations. These were used in the biocompatibility and drug release studies to enable faster degradation than PEGDA alone, whilst maintaining some structural integrity.

Drug Release: A cardiovascular disease hypertension active, trandolapril, was used as a model drug in drug release screening from candidate formulations (see supplementary). Here, the χ parameter was used to predict which ink component trandolapril has more affinity with and would migrate toward (**Table S6**). With PEGDA alone, **Figure 2C**, we observed that the fastest release profiles were those from PCLMA/PEGDA and PTMC/PEGDA, each of which presented a core-shell microstructure in the SDS. PTMCMA/PEGDA exhibited the next fastest release and presented a dispersed droplets microstructure. In each of these cases, χ analysis predicted that trandolapril had more affinity for and would migrate toward the PEGDA (**Table S6**). In contrast PTMCMAA/PEGDA, PLAMA/PEGDA and PLA/PEGDA had significantly slower release, and χ forecasted greater active affinity for the oligomers over PEGDA, suggesting that the release is significantly slowed due to hydrophobicity of these materials. Therefore, we hypothesized that when using PEGDA alone, cast drug release rates are predominantly controlled by their affinity for PEGDA and that the microstructure provides a secondary tuning parameter. In contrast, all formulations with PEGDA/NVP, with the sole exception of PTMCMAA, exhibited very similar dissolutions rates which were seemingly unaffected by the microstructure, i.e. the drug release appeared to be dominated by the PVP behaviour. The AFM and optical images of the PTMCMAA/PEGDA/NVP formulation surfaces indicate segregation behavior quite unlike those observed in other formulations, suggesting a complex set of interactions that may be leading to exceptional drug release behavior.

Macro-scale 3D ink-jet printing of drug eluting samples

The SDS and cast samples evaluation were used to guide the choice of materials for 3D ink-jet printed drug releasing devices. Our screens indicated that two “levers” controlled deposition for an API, namely NVP inclusion and microstructure. Thus, we chose formulations predicted to show a range of release rates and therefore were guided by the release from cast materials (leading to the addition of NVP to PCLMA/PEGDA, and PTMCMA/PEGDA) and also by the SDS and degradation data (leading to use of PLAMA/PEGDA/NVP). We also incorporated a second active, the cholesterol lowering drug pitavastatin, into these formulations to demonstrate the predictions’ effectiveness for multiple actives. Pitavastatin offers an effective contrast since it has a similar log P to trandolapril (3.97 and 3.45 respectively) but different aqueous solubility (0.426 mg/L and 2.5 mg/L respectively). The amount of drug released from 3D printed constructs was quantified on day 3, 15, 30 and 60, and 3D OrbiSIMS was used to unambiguously identify each compound^[13] (**Figure S11**) and ToF-SIMS micro-scale resolved maps of bulk composition (via depth analysis) were used to understand the role of phase separation on drug distribution and release (**Figure 3B**).

Drug release and ToF-SIMS assessment showed that both PCLMA/PEGDA and PTMCMA/PEGDA constructs exhibited similar extended-release profiles and material distributions within the construct (**Figure 3B**). The latter were similar to those observed in the SDS microarray, indicating its reliability in predicting 3D printed material separation. ToF-SIMS (**Figure 3B**) also confirmed the affinity between the API and the PEGDA within a formulation, as we predicted from the χ values (**Table S6**). This indicated that microstructure dominated the drug release behavior in these printed samples, with the release likely via

diffusion from exposed PEGDA, whilst also suggesting that the SDS, cast and printed samples have the same microstructure.

Using PCLMA, PTMCMA and PLAMA oligomers with NVP/PEGDA resulted in a range of drug release profiles that broadly followed the degradation rates of the core polymers. We noted that PCLMA/PEGDA/NVP's release was not statistically different to that from PCLMA/PEGDA, whilst using PTMCMA resulted in a substantial increase and PLAMA gave full release in < 20 days. This behavior, in combination with insights from ToF-SIMS 3D mapping (**Figure S12, Figure 3B**) leads us to propose that, whilst cast samples are not a reliable guide to release when using NVP, the similarity in microstructure in SDS and 3D printed samples indicates the reliability of SDS as a guide to performance when manufacturing via printing. In each case (with or without NVP) the microstructure is a determining factor, but via a different mechanism. When using NVP, ToF-SIMS confirmed that the drug and PVP are homogeneously distributed, as expected when using χ values to inform PVP:drug compatibility. Thus, the release is driven by PVP dissolution rather than diffusion of the drug within the PVP and will be controlled by the extent of the exposed PVP, a feature dependent on the microstructure. This degradation is also dependent on the oligomer degradation speed, i.e. rate of exposure of further PVP surface area, leading to the rapid release seen when using PLAMA (**Figure 2A**).

Conclusions

We have shown that the microstructure formed in our polymer blends was process dependent and arose as a function of the drop-by-drop deposition technique. As a result, we demonstrated that it is possible to functionally tailor the composition of 3D printed constructs to successfully control the release of drugs incorporated within them. We selected suitable 3D printing inks using complementary HTP methodologies that allowed us to screen for various

desired properties and down select formulations from these screens. Screening of behavior in single drops, combined with the Flory-Huggins interaction parameter provided a prediction of phase separation, and thus drug release, in 3D printed structures. In summary, we demonstrated a reliable toolkit for the development of formulations suitable for 3D printing that can be used to tailor long term drug release on demand.

Acknowledgments

This work was principally funded by the Engineering and Physical Sciences Research Council grant EP/N024818/1. Additional support came from EP/P031684/1 (GT), EP/L015072/1 (FR) and EP/N006615/1 (VT, LB), EP/P029868/1 (GT). Open access funding was provided by UK Research and Innovation. The manuscript was written with contributions of all authors. The majority of the experimental and characterization work was conducted by LR with 3D printing support from EC, RW, CT and RH, chemical synthesis support from VT and DI, and cell culture facilities and guidance provided by FR. Materials characterisation was supervised by CR and DI and the HTP performed by ZZ and LB and overseen by RW and MA. OrbiSIMS work was performed by GTF supervised by CR. The work was conceived and organised by DI and RW.

References

- [1] P. Darney, A. Patel, K. Rosen, L. S. Shapiro, A. M. Kaunitz, *Fertil. Steril.* **2009**, *91*, 1646.
- [2] A. Malclès, C. Dot, N. Voirin, A.-L. Vié, É. Agard, D. Bellocq, P. Denis, L. Kodjikian, *RETINA* **2017**, *37*.
- [3] D. L. Citrin, M. I. Resnick, P. Guinan, N. Al-Bussam, M. Scott, T. C. Gau, G. T. Kennealey, *Prostate* **1991**, *18*, 139.

- [4] H. de N. Oss, *Contraceptive Implant*, **1990**, US4957119A.
- [5] V. Wong, F. Kochinke, *Formulation for Controlled Release of Drugs by Combining Hydrophilic and Hydrophobic Agents*, **1999**, 5869079.
- [6] M. Kyobula, A. Adedeji, M. R. Alexander, E. Saleh, R. Wildman, I. Ashcroft, P. R. Gellert, C. J. Roberts, *J. Control. Release* **2017**, *261*, 207.
- [7] S. A. Khaled, M. R. Alexander, R. D. Wildman, M. J. Wallace, S. Sharpe, J. Yoo, C. J. Roberts, *Int. J. Pharm.* **2018**, *538*, 223.
- [8] B. D. Ulery, L. S. Nair, C. T. Laurencin, *J. Polym. Sci. B. Polym. Phys.* **2011**, *49*, 832.
- [9] L. Ruiz-Cantu, A. Pearce, L. Burroughs, T. Bennet, C. Vasey, R. Wildman, D. Irvine, C. Alexander, V. Taresco, *Macromol. Chem. Phys.* **2018**, *220*, 1800459.
- [10] K. Fukushima, *Polym. J.* **2016**, *4880*, 1103.
- [11] I. Louzao, B. Koch, V. Taresco, L. Ruiz Cantu, D. J. Irvine, C. J. Roberts, C. J. Tuck, C. Alexander, R. J. M. Hague, R. D. Wildman, M. R. Alexander, *ACS Appl. Mater. Interfaces* **2018**, DOI 10.1021/acsami.7b15677.
- [12] Z. Zhou, L. Ruiz Cantu, X. Chen, M. R. Alexander, C. J. Roberts, R. Hague, C. Tuck, D. Irvine, R. Wildman, *Addit. Manuf.* **2019**, *29*, 100792.
- [13] M. K. Passarelli, A. Pirkl, R. Moellers, D. Grinfeld, F. Kollmer, R. Havelund, C. F. Newman, P. S. Marshall, H. Arlinghaus, M. R. Alexander, A. West, S. Horning, E. Niehuis, A. Makarov, C. T. Dollery, I. S. Gilmore, *Nat. Methods* **2017**, *14*, 1175.

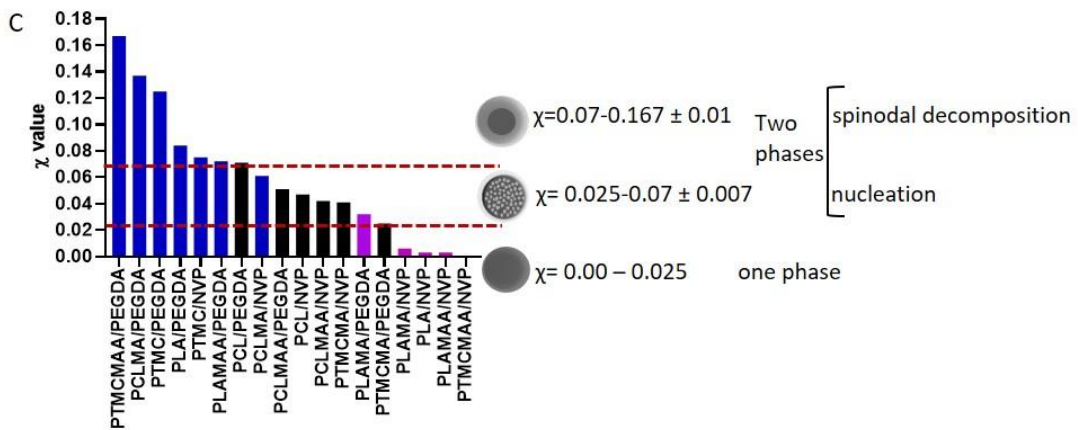
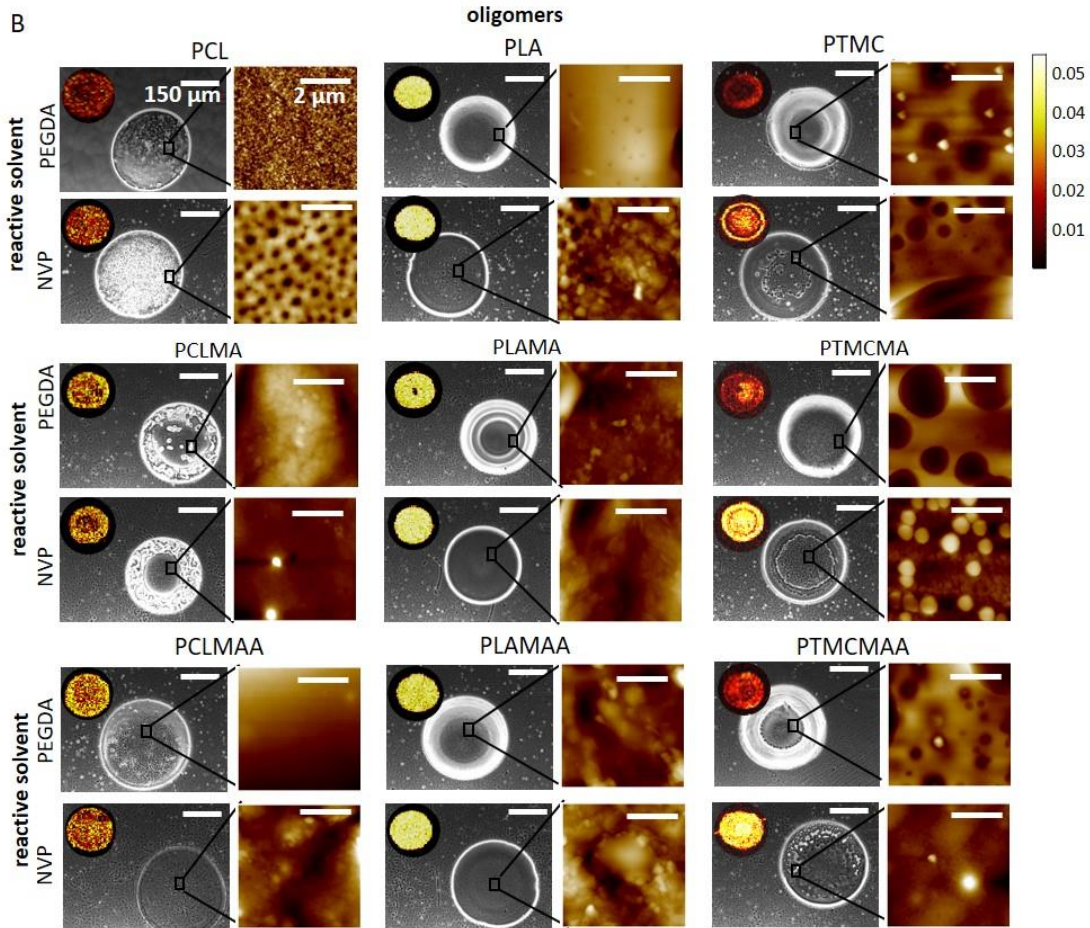
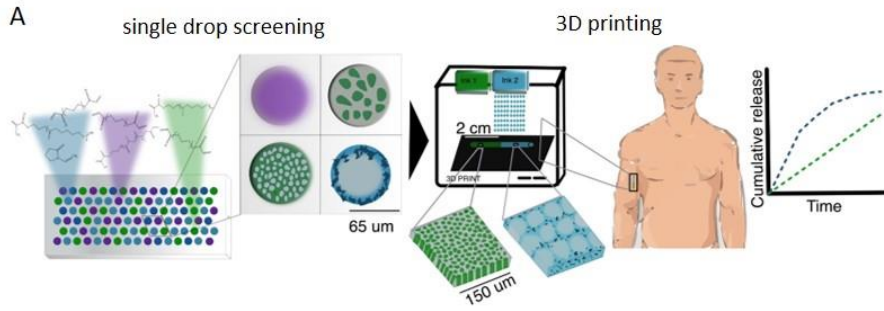


Figure 1. Design toolkit, χ values, microscopy, ToF SIMS ion (top left of images) and AFM topographical images of eighteen different spots from the microarray representing a single voxel of printed ink. (A) Schematic representation of the design toolkit for the screening and selection of inks for 3D printing personalized implants. (B) Microscopy images, topographical AFM images and ToF SIMS images from the from eighteen different macromer/reactive solvent combinations spots. Scale bars on the microscopy images represent 150 μm . Scale bars on AFM images represent 2 μm . ToF SIMS ion images represent the positive ions $\text{C}_6\text{H}_{10}\text{O}_2^+$ for PCL, $\text{C}_3\text{H}_4\text{O}_2^+$ for PLA and $\text{C}_4\text{H}_7\text{O}_3^+$ for PTMC derived materials. (C) Phase separation taxonomy based on χ values and microstructure morphologies from the spots.

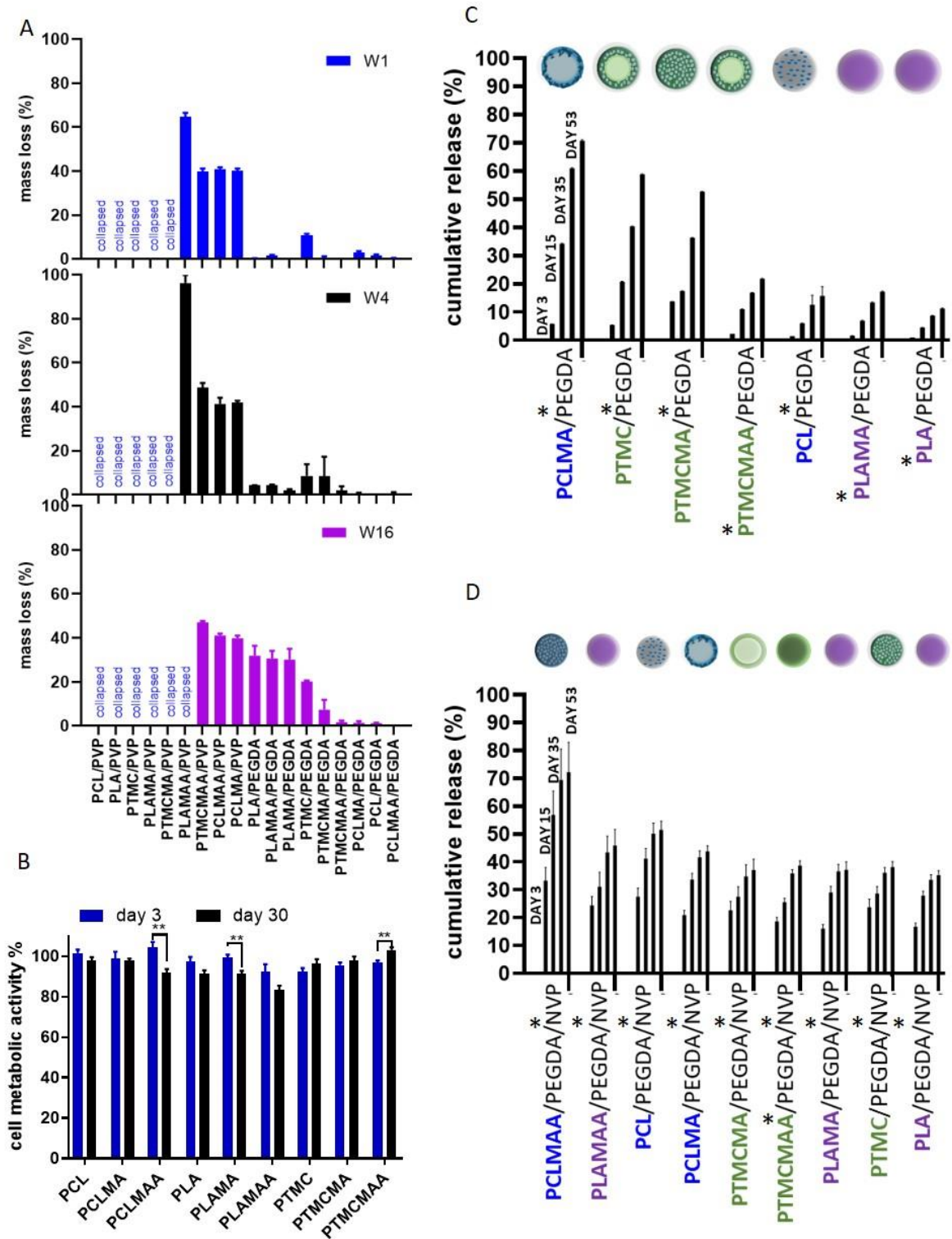


Figure 2. HT screening of the base macromers combined with the two different reactive solvents. (A) Mass loss and structural stability screening on weeks 1, 4 and 16. The samples marked as collapsed are the ones that swelled, then lost structural stability and collapsed into powder ($n=3$, \pm SD). (B) Materials cytotoxicity represented as cell metabolic activity of the cells after indirect contact test ($p=0.006$, two-way ANOVA with Tukey test, $n=3$, \pm SD). (C)

Cumulative release of trandolapril from oligomer:PEGDA samples over a period of 53 days. (D) Cumulative release of trandolapril from oligomer:PEGDA/NVP samples over a period of 53 days powder ($n=3, \pm SD$). The schematics in the graphs represent the phase separation on the materials observed on the droplets. The asterisk represents the component of the ink that trandolapril has more affinity with according to the χ values.

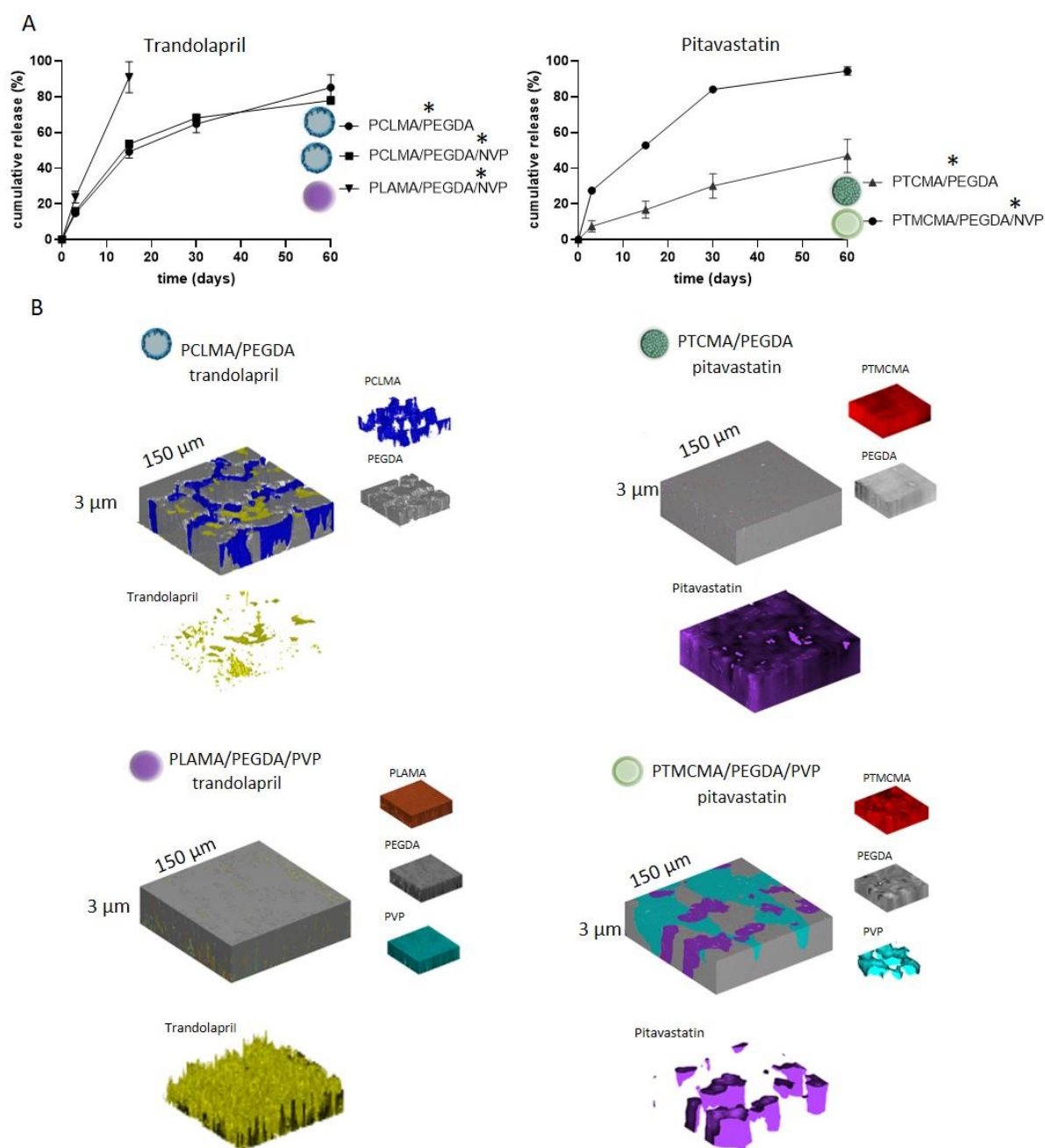


Figure 3. 3D printed formulations containing the API trandolapril and pitavastatin with tuned release profiles. (A) Release profiles of the different 3D printed formulations containing trandolapril and pitavastatin for a period of 60 days ($n=3, \pm SD$). The asterisk represents the

component of the ink that trandolapril or pitavastatin has more affinity with according to the χ values. (B) 3D reconstruction of ToF SIMS depth profiles showing the phase separation represent the negative ions PCLMA ($C_4H_5O_3^-$) PLAMA ($C_3H_3O_2^-$), PTMCMA ($C_4H_5O_3^-$), PEGDA ($C_2H_3O^-$), PVP ($C_4H_6NO^-$), trandolapril ($C_{24}H_{33}N_2O_5^-$) and pitavastatin ($C_{20}H_{15}FN^-$).

Supporting Information

Formulation induced microstructural control of 3D printed polymers derived from oligomer libraries: controlling drug release for personalized subdermal implants

Laura Ruiz-Cantu, Gustavo F. Trindade, Vincenzo Taresco, Zuoxin Zhou, Laurence Burroughs, Elizabeth Clark, Felicity R. A. J. Rose, Morgan Alexander, Christopher Tuck, Richard Hague, Clive Roberts, Derek J. Irvine and Ricky D. Wildman**

**Derek.Irvine@nottingham.ac.uk*

**Ricky.Wildman@nottingham.ac.uk*

Experimental Section

Materials. D,L-lactide 99% was purchased from Alfa Aesar (by Thermo Fisher Scientific). Trimethylene carbonate (TMC) was purchased from Polyscience. ϵ -caprolactone, extra dry dichloromethane (DCM), deuterated chloroform (CDCl_3), acrylic acid, hydroxyethylmethacrylate (HEMA), benzyl alcohol, poly(ethylene glycol) diacrylate 250, N-vinyl-2-pyrrolidone (>99%), 4-Dimethylaminopyridine and triazabicyclodecene (TBD) were acquired from Sigma Aldrich. Hexane, diethyl ether, N,N-dimethylformamide (DMF) and methanol were obtained from Fisher. Trandolapril and pitavastatin were purchased from Carbosynth. In all cases the vials were dried in an oven at 50 °C overnight prior to use, and the HEMA and DCM were stored over molecular sieves and under an inert atmosphere.

Benzyl alcohol (BA) and hydroxyethylmethacrylate (HEMA) initiated ROP of the

oligomers. The oligomers were synthesized by ring opening polymerization using metal free organocatalysis,^[1] chosen for low toxicological impact of any subsequent medical devices.^[2] ROP experiments were performed adopting ‘standard laboratory’ conditions, i.e. ambient temperature and atmosphere.^[3] -OH ended macromers were initiated using BA, -MA and MA-A macromers were initiated using HEMA. Macromers were synthesized following the procedure by Ruiz et al ^[1]. Briefly, 1000 mg of cyclic monomer (caprolactone, lactide or trimethylene carbonate) and BA or HEMA ($[\text{M}]:[\text{I}]$ or DP_0 ratios targeted to produce final molar masses of 5000 Da were weighed into a vial, which had been dried in an oven at 50 °C overnight and capped with a rubber septum. DCM (5 ml), was then added via syringe and the mixture was allowed to dissolve at room temperature (RT) for 5-10 minutes. Varying amounts of catalyst (1% mol/mol of TBD for lactide and trimethylene carbonate, 2 % mol/mol of TBD for caprolactone) were then added to trigger the ring-opening process.

Reactions were observed to occur in time-frames ranging from 15-120 minutes, according to the monomer:initiator :solvent :catalyst adopted ratios. The reaction was terminated by catalyst deactivation upon adding an acidic solution and the polymer purified by means of multiple precipitation steps and dried in a vacuum oven.

MA-A macromers end capping. The MA-OH macromers were further functionalized with an acrylate end using a Stenglich coupling esterification following the same procedure by Taresco, et al^[4]. Briefly, PCLMA, PLAMA or PTMCMA (0.2 mmol) and DMAP (0.04 mmol) were added to DCM (5 ml) at room temperature in a glass vial under magnetic stirring until complete dissolution. A second solution was prepared by dissolving 1 mmol of EDC and 1 mmol of acrylic acid in 2 ml of DCM. After dissolution, both solutions were mixed. The reaction was allowed to stir for 48 hours. The modified macromers were purified under multiple precipitation steps and dried in a vacuum oven.

¹H NMR spectroscopy. ¹H NMR spectra were recorded on a Bruker AV3400 400.1 MHz spectrometer using CDCl₃ as the solvent reference (7.26 ppm). Chemical shifts are expressed in parts per million (d) downfield from internal standard tetramethylsilane.

PCLMA: ¹H NMR: (400 MHz, CDCl₃): δ 6.14 (s, 1H), 5.61 (s, 1H), 4.40-4.30 (m, 4H), 4.08 (t, 2H*[M]:[I]), 3.68 (m, 2H), 2.33 (t, 2H*[M]:[I]), 1.97 (m, 3H), 1.67 (m, 4H*[M]:[I]), 1.41 (m, 2H*[M]:[I])

PLAMA: ¹H NMR (400 MHz, CDCl₃): δ 6.14 (s,1H), 5.61 (s, 1H), 5.19 (t, 2H*[M]:[I]), 4.36 (m, 5H), 1.95 (m, 3H), 1.59 (m, 6H*[M]:[I])

PTMCMA: *1H NMR* (400 MHz, CDCl₃): δ 6.14 (s, 1H), 5.61 (m, 1H), 4.39 (m, 4H), 4.25 (m, 4H*[M]:[I]), 3.74 (m, 2H), 2.04 (m, 2H *[M]:[I]), 1.96 (m, 3H)

PCLMAA: *1H NMR*: (400 MHz, CDCl₃): δ 6.64 (s, 1H), 6.29 (s, 1H), 6.14 (s, 1H), 5.61 (s, 1H), 5.59 (s, 1H) 4.40-4.30 (m, 4H), 4.08 (m, 2H*[M]:[I]), 3.68 (m, 2H), 2.33 (m, 2H*[M]:[I]), 1.97 (m, 3H), 1.67 (m, 4H*[M]:[I]), 1.41 m, (2H*[M]:[I])

PLAMAA: *1H NMR* (400 MHz, CDCl₃): δ 6.64 (s, 1H), 6.29 (s, 1H), 6.14 (s, 1H), 5.61 (s, 1H), 5.59 (s, 1H), 5.19 (m, 2H*[M]:[I]), 4.36 (m, 5H), 1.95 (m, 3H), 1.59 (m, 6H*[M]:[I])

PTMCMA: *1H NMR* (400 MHz, CDCl₃): δ 6.64 (s, 1H), 6.29 (s, 1H), 6.14 (s, 1H), 5.61 (s, 1H), 5.59 (s, 1H), 4.39 (m, 4H), 4.25 (m, 4H*[M]:[I]), 3.74 (m, 2H), 2.04 m, (2H *[M]:[I]), 1.96 (m, 3H)

Materials library preparation

Our library of inks was composed of a new set of biodegradable, UV curable materials, which were screened using high throughput methodologies to identify key characteristics suitable for use as an implant, such as printability, biodegradability, cytotoxicity and drug elution (**Figure S1**). The library was created by combining the nine hydrophobic macromers with two different relative hydrophilic reactive solvents in a 1:1 ratio (w/v) resulting in a total of 18 inks. The solvents functioned as diluents and cross-linkers. Polyethylene glycol diacrylate (PEGDA) 250 Mw and n-vinyl pyrrolidone (NVP) were chosen as the reactive solvents. PEGDA is commonly used as a plasticizer to reduce the glass transition temperature of polymers such as PLA,^[5] which helps reduce viscosity without the need of using high temperatures. It is also non-degradable so will not be depleted from the structure. Meanwhile, NVP was selected because once polymerized into poly(*N*-vinylpyrrolidone) (PVP) it has the ability to form a water-soluble composite structure with insoluble active substances and

improve the release and solubility of drugs.^[6,7] Additionally, NVP is also known to increase the reactivity of acrylate resins^[8] and will degrade in hydrolytic conditions so be removed from any printed structure during use. All the formulations were a 50% w/v solution of the macromer (s) in the solvent (s). Whilst the reactive solvents both functioned as diluents, NVP is monofunctional so gives rise to linear polymer chains and PEGDA is difunctional so functions as a cross-linker/branching monomer so giving rise to a 3D network structure. Additionally, both were chosen as the reactive solvents because they are commonly used in pharmaceutical formulations owing to their ability to interact with hydrophilic and hydrophobic solvents, polymers and drugs,^[9,10] and they exhibit different degradation behavior. Formulations contained 1% Irgacure 2959 as photoinitiator.

Microarray preparation.

DMF (75% w/v) was used as a non-reactive solvent for all the formulations in this experiment in order to study their properties in high throughput without the need to optimize viscosity in advance. The microarrays were prepared on polyHEMA coated glass slides using the using XYZ3200 dispensing station (Biodot) and quilled metal pins (946MP6B, Arrayit) under argon atmosphere (< 2000 ppm oxygen) maintaining between 40 and 50% relative humidity. Each spot had an average diameter of 200 μm . The spots were UV polymerized under argon atmosphere for 10 min after printing. To remove the solvent, glass slides were dried the in vacuum oven for a week.

Atomic Force Microscopy. Height, Peak Force error, DMT modulus, logDMT modulus, adhesion, deformation and dissipation images were simultaneously acquired by Peak Force QNM-AFM measurements (Bruker Fast Scan). Images of 5x5 μm per spot were recorded by

using a programmable stage. AFM cantilevers with a nominal stiffness nominal $k= 40$ N/m (RTESPA 300) were used. A Poisson's ratio of 0.3 was used in all cases. Three images were acquired per polymer spot throughout the micro array. The spring constant of each cantilever was estimated by using the thermal tune. Sample standards of polystyrene (PS) were also used to validate tip characterization. Images were analyzed using the NanoScope Analysis software.

ToF SIMS: ToF-SIMS of microarray samples was carried out using a TOF.SIMS IV instrument from IONTOF GmbH (Muenster, Germany). ToF-SIMS analysis of positively charged secondary ions was carried out using a TOF.SIMS IV system from IONTOF GmbH (Münster, Germany) using 25 keV Bi_3^+ ion beam operated in the high current bunched mode delivering 0.3 pA with 100 μs cycle time, resulting in a mass range between 0 and 694 u. Secondary ion maps were acquired using the stage raster mode. The whole area was scanned once with one shot per pixel, ensuring static conditions.

Flory-Huggins interactions parameter. To investigate the phase separation in pin printed droplets, we used a combination of the Flory-Huggins theoretical model and experimental characterization methods. The Flory–Huggins parameter (χ) describes the excess free energy of mixing and governs phase behavior for polymer blends and block copolymers^[11]. In order to calculate the χ value we first obtained the Hansen solubility parameter of the individual components of the formulation using the HSPiP program, where the δ_d , δ_p , δ_h and δ_{TOT} were obtained using the DYI tool of the software. We calculated the χ values following the procedure described by Imre et al.^[12] by using equation 1,

$$\chi = \frac{V_r}{RT} (\delta_1 - \delta_2)^2 \quad (\text{equation 1})$$

where V_r is the molar volume of the repeating unit of the oligomer, R is the gas constant, T the absolute temperature and δ_1 and δ_2 are the total solubility parameter (δ_{TOT}) of the solvent and the oligomer respectively.

The phase separation taxonomy was created from observations from the printed spots and the χ values. The boundaries were chosen such that we included all the samples that exhibited the dispersed droplet phenomena. This resulted in two exceptions that showed either core-shell or homogeneous microstructure, which reflected the fact that the boundaries were not hard, and could be influenced by other physical properties such as viscosity and curing rate; we estimated the likely error in the boundary by calculating the average difference between χ at the boundary and at the exceptions, resulting in an approximate error of ± 0.01 .

Printability screening. To investigate the printability of the inks we used a HT method developed by Zuoxin et al^[13] where the viscosity and surface tension are measured using a liquid handler and the printability calculated using the Ohnesorge number ($Z=1/Oh$). The Ohnesorge number has been identified as the appropriate grouping of constants to characterize drop formation^[14]. Reis & Derby used numerical simulation of drop formation to propose $10 > Z > 1$ for stable drop formation^[15]. To identify printability at different temperatures, eighteen based inks formed by the combination of the nine different macromers mixed with PEGDA and NVP were selected and screened using ranges from 40 °C to 70 °C.

Degradation. This study was performed on the 18 primary inks. Cast cylindrical samples with dimensions of 4 mm length and 1 mm radius were used for this test. The samples were prepared by transferring 15 μ l of each ink into a 4 mm piece of silicone tubing, then placed under UV for 3 minutes for crosslinking. Triplicates of each sample were prepared for each

of the timepoints. Samples were transferred to individual vials containing 5 ml of phosphate buffered saline solution and placed in an incubator at 37 °C. Triplicates of each sample were weighed, vacuum dried and weighed again at week 1, 4, 8 and 16 to calculate the mass loss at each time point.

Degree of conversion. Samples were analyzed with a Perkin Elmer Frontier FTIR-ATR spectrometer (Seer Green, UK) from 4000 cm^{-1} to 600 cm^{-1} with a scan resolution of 2 μm and step size of 0.5 cm^{-1} . Three scans were collected for each sample. Prior to sample spectrum collection, a background was collected on the clean ATR crystal. The degree of curing was calculated by quantifying the reduction of the C=C acrylate stretches (1636 cm^{-1}) and the CH² acrylate twist 810 cm^{-1} when the macromers were combined with the reactive solvent PEGDA. The degree of conversion of on the samples mixed with NVP was calculated by looking at the reduction of the C=C vinyl groups of the NVP (1639 cm^{-1}).

Cytotoxicity (Extract test). To test biocompatibility (**Figure 2B**), we performed an indirect cytotoxicity test for a period of 30 days to determine any evolving cytotoxicity of leached products, either through residual monomers or products emerging through polymer degradation. BJ6 fibroblasts were grown in Dulbecco's modified eagle medium (DMEM) supplemented with 10% (v/v) foetal calf serum, 1 % MEM non-essential amino acids solution (Sigma-Aldrich), and 1% antibiotics/antimycotics (100 units/mL penicillin, 100 mg/mL streptomycin, and 0.25 mg/ml amphotericin B; Life Technologies). Cells were cultured until they reached 80% confluency and subsequently detached from the culture surface using trypsin/EDTA (0.25%/0.02% w/v), centrifuged at 200 x g for 5 min and resuspended in culture medium. Cells were seeded in a 96 well plate at a density of 5,000 cells per well and

allowed to attach for 24 hours before the cytotoxicity experiments. A new seeded well plate was used for each time point.

Triplicates of each formulation cast samples were sterilized under UV light (0.05 mW/cm², 265nm) for 50 minutes and transferred into a 48-well plate. Each well containing a sample was filled with 1 ml of culture medium. Samples were incubated in the medium for a total of thirty days to allow for leaching of any cytotoxic components. After day 1, day 3 and day 30 of incubation, 200 µl of the supernatant were transferred in triplicate to the cells seeded in the 96-well plates. Cells cultured in in standard medium were used as negative control. Cells were incubated for 24 hours with the supernatant with cells cultured in fresh culture medium used as a negative control. Cytotoxicity was measured using Presto Blue™ (Invitrogen) following the manufacturer's instructions. The fluorescent signal was measured with an automated microplate reader (Tecan) using an excitation wavelength of 560 nm and an emission wavelength of 590 nm. For the cytotoxicity percentage calculations, the fluorescent background control was first subtracted from all the samples. Then the percentage was calculated by multiplying the fluorescence of each sample by 100 and then dividing the total by the average fluorescence of the negative control.

Drug release study. The drug release profile was screened for a period of eight weeks on 16 of the formulations, with PCLMAA/PEGDA and PLAMAA/PEGDA being eliminated as they were not within the printable range. The drug trandolapril was selected for this screening. Formulations containing 0.65% w/v of trandolapril were casted in the same way than for the degradation study. Samples were transferred to individual vials containing 3 ml of phosphate buffered saline solution and placed in an incubator at 37°C. 500 µl of the PBS solution were collected and each timepoint and filtered (0.45µm) for the HPLC analysis. The

PBS solution was refreshed at each timepoint. For the drug release studies of the 3D printed samples the formulation were prepared in the exact same way than the cast ones.

HPLC. Samples were characterized with an Agilent (Santa Clara, USA) HPLC Series 1260 system, equipped with an auto sampler, degasser, UV lamp and multi-diode array detection. A wavelength of 210 nm was used to quantify trandolapril and 280 nm for pitavastatin. Method mobile phase compositions were 65% phosphate buffer and 35% acetonitrile (Fisher HPLC gradient grade). Phosphate buffer was composed of 6.8 g/L monobasic potassium phosphate (anhydrous, Sigma Aldrich) adjusted to pH 3.0 with phosphoric acid (85–90%, Fluka). An Ultimate LP-C18 column (5 μ m, 25 cm \times 4.6 mm diameter) was used to separate the samples at 40 °C. A flowrate of 1 mL/min using a 10 μ L injection volume was implemented; runtime was 10 min. Trandolapril stock solutions were prepared by sonicating trandolapril/pitavastatin (nominally 1 mg, Carbosynth) in 10 mL methanol (Fisher HPLC grade) and diluting the volume with dissolution media in a 10 mL volumetric flask. Standards were prepared with the stock solution and dissolution media.

Printing. The formulations were printed using a Dimatix Materials printer (DMP-2830 Fujifilm). The printer was enclosed in a metallic environment box and filled with nitrogen gas. The oxygen level was kept between $0.25 \pm 0.05\%$ during the printing process to minimize the inhibition effect caused by oxygen during the free radical photo-polymerization curing procedure. A 10pL disposable printhead, Dimatix Materials Cartridge (DMC-11610, Fujifilm) was used for printing. In-line UV curing was applied at the cartridge height immediate after each swath of ink droplets are deposited, by using a LED UV unit (365nm, 800mW/cm², Printed Electronics Limited, Tamworth, UK) attached and move with the printhead unit. The printing temperature was set to 28°C. The sample was printed at 30 μ m

for the first layer and reduced to 20 μm for all the following layers. The height of the printhead was set to 700 μm with an increment of 9 μm after each layer printed.

The samples were 3D printed using an inkjet printer (Dimatix DMP 2800) on the hydrophobic substrate polyethylene naphthalate. Samples dimensions were 5x5x 1 mm. Individual sessile droplet size when deposited varied depending on the mixture being processed.

ToF-SIMS of printed samples was carried out using a 3D OrbiSIMS (hybrid SIMS) instrument from IONTOF GmbH (Muenster, Germany). Secondary ion mass spectra were acquired in negative ion polarity with delayed extraction mode using a 30 keV Bi_3^+ primary ion beam delivering 0.3 pA. The ToF analyser was set with 200 μs cycle time, resulting in a mass range between 0 and 3493 mass units. For the surface spectra, the primary ion beam was raster scanned over different areas with the total ion dose kept under the static limit of 10^{13} ions/ cm^2 . The 3D depth profiling data were acquired in dual-beam mode by raster scanning the primary ion beam over regions of up to 150 x 150 μm^2 at the centre of 300 x 300 μm^2 sputter craters formed using an argon gas cluster ion beam (GCIB). The GCIB was operated with 20 keV and 2000 atoms in the cluster delivering a pulsed 5 nA beam current. The analysis was performed in the “non-interlaced” mode with a low-energy (20 eV) electron flood gun employed to neutralise charge build up. 3 sputter frames were performed per cycle with 15 analysis scans per cycle and a pause time in between cycles of 0.5 s. Optical profilometry was used to determine the crater depth after ToF-SIMS depth profiling experiments and calibrate the depth scale. Scans were obtained using a Zeta-20 optical microscope (Zeta Instruments, CA, USA). All maps were produced using SurfaceLab and 3D visualisations were produced using the simsMVA software^[16]. Intensities were

normalised by total ion counts to correct for topographic features. The final 3D representations were created by combining rendered isosurfaces ranging from 40% to 90% of the maximum normalised intensity for each ion.

orbiSIMS of a cross section of a multi-layer printed sample containing all compounds of interest was carried out using a 3D orbiSIMS (hybrid SIMS) instrument^[17] A 20 keV Ar_{3000}^+ imaging GCIB of 5 μm diameter was used as primary ion beam, delivering 18 pA (with duty cycle set to 37.7%). Images were acquired over an area of $263 \times 263 \mu\text{m}^2$ using random raster mode. Optimal target potential was set to -292 V. Argon gas flooding was used to aid charge compensation. The images were collected in negative polarity, in the mass range of 75-1125 m/z . The injection time was set to 511 ms. Mass resolving power was 243000 at 200 m/z .

Statistical analysis. Statistical analysis was performed using Prism version 8.0 (GraphPad Software, USA). Statistical significance was determined by two-way ANOVA followed by a Turkey test. Plots are means with error bars indicating the standard error. Statistically significant values are presented as * $p < 0.05$, ** $p < 0.01$, *** $p < 0.001$ and **** $p < 0.0001$.

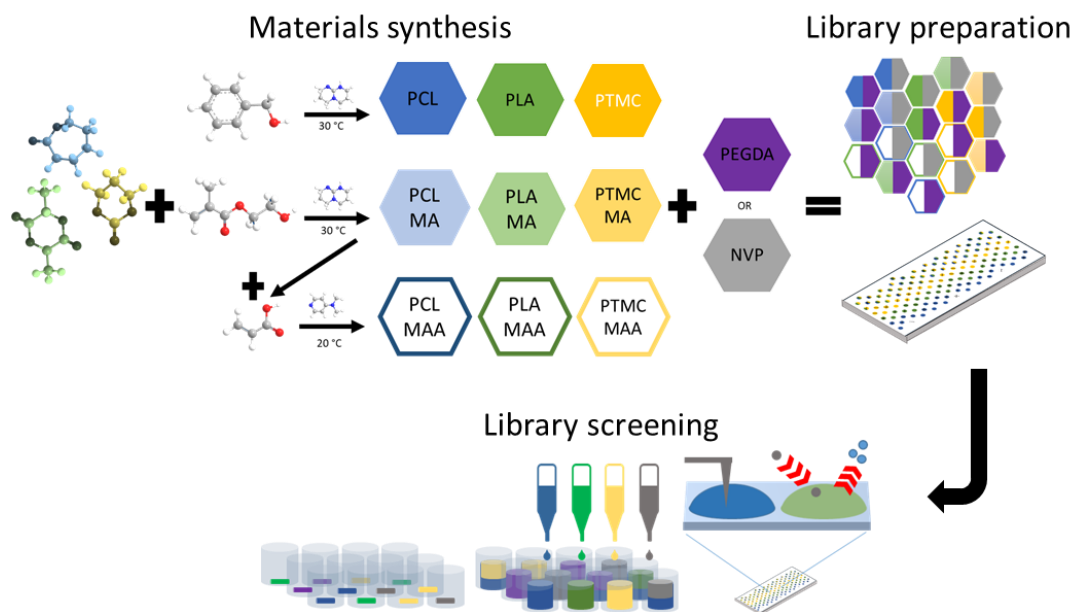


Figure S1. Schematic representation of the process for the rapid synthesis and screening of printable biodegradable materials. Starting by materials synthesis, followed by the library formulation and HTP screening of microstructure, biodegradation, cytotoxicity, degree of conversion and drug release.

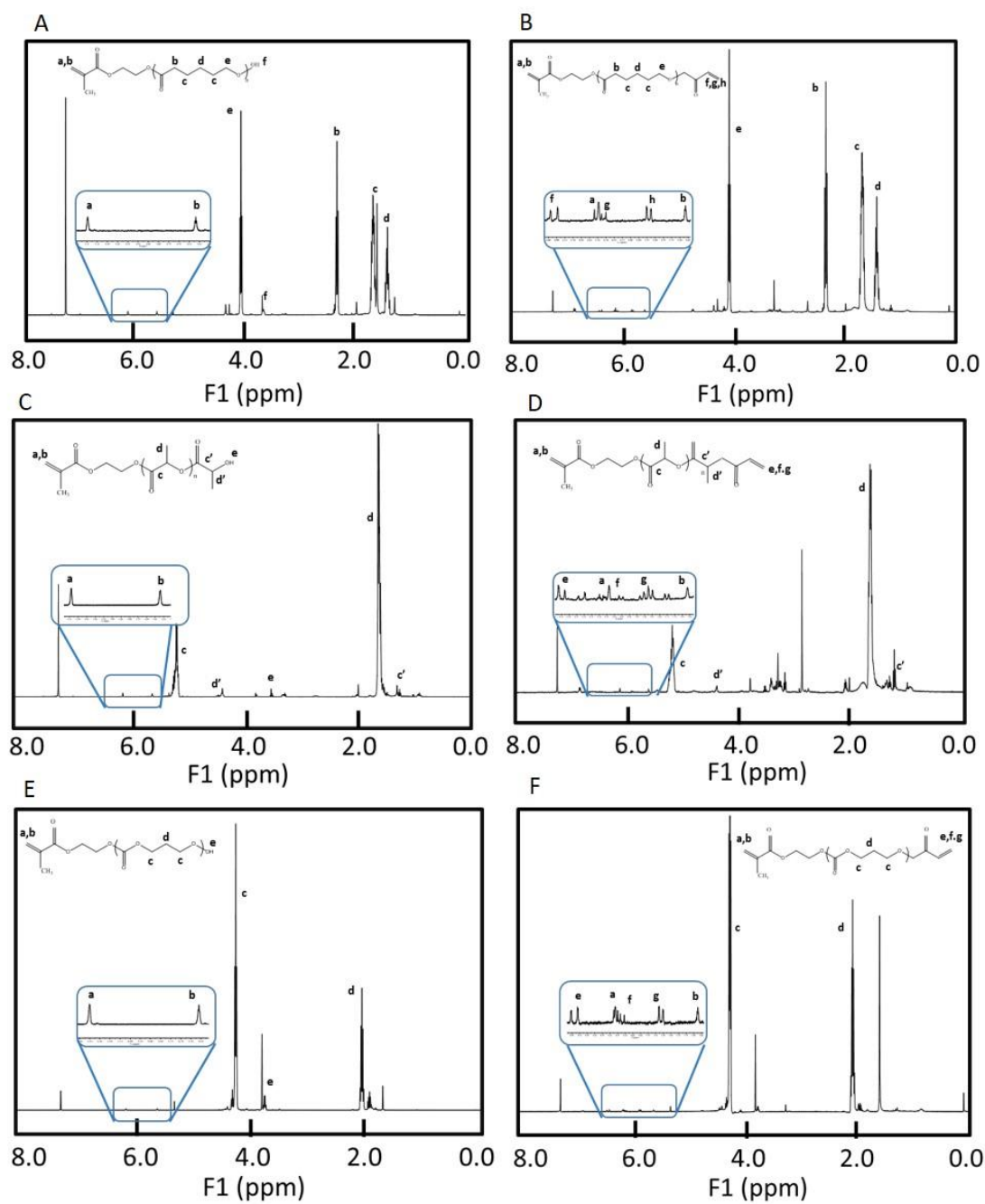
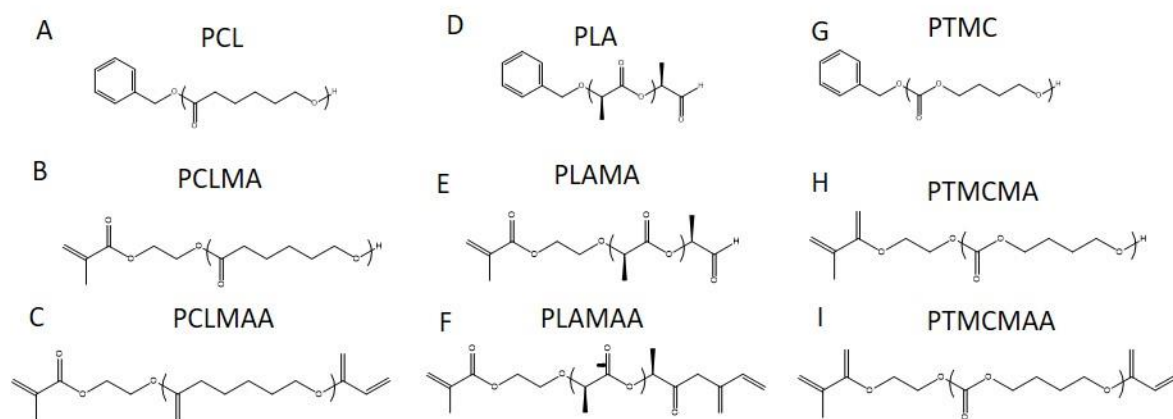


Figure S2. ^1H NMR spectrum of the obtained macromers (A) poly (caprolactone) methacrylate, (B) poly (caprolactone) methacrylate acrylate, (C) poly (D,L-lactic acid) methacrylate, (D) poly (D,L-lactic acid) methacrylate acrylate, (E) poly (trimethylene carbonate) methacrylate and (F) poly (trimethylene carbonate) methacrylate acrylate in CDCl_3

base materials



reactive solvents

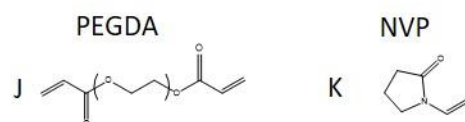


Figure S3. Chemical structures of the base materials and reactive solvents. (A) poly (caprotacone), (B) poly (caprolactone) methacrylate (C) poly (caprolactone) methacrylate acrylate, (D) poly (D,L-lactic acid), (E) poly (D,L-lactic acid) methacrylate, (F) poly (D,L-lactic acid) methacrylate acrylate (G) poly (trimethylene carbonate), (H) poly (trimethylene carbonate) methacrylate, (I) poly (trimethylene carbonate) methacrylate acrylate, (J) poly ethylene glycol and (K) n-vinylpyrrolidone.

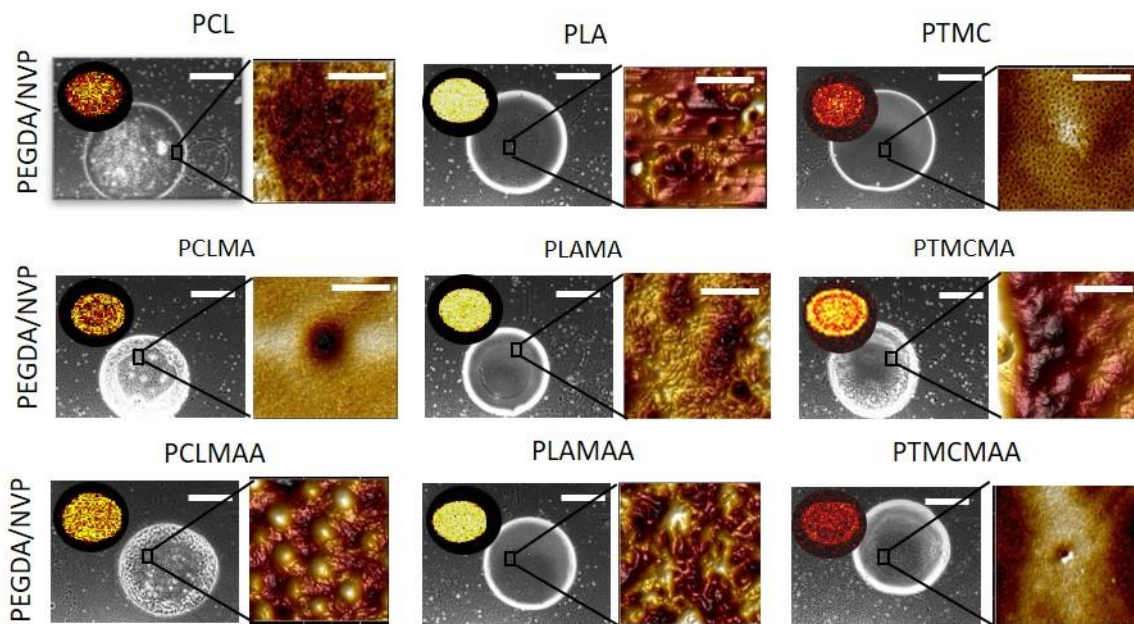


Figure S4. 3D visualization AFM images representing the surface of the spots. Each image is $5 \times 5 \mu\text{m}$.

Table S1. Values used for the calculation of the Flory-Huggins interaction parameter (χ)

material	molar mass	density	molar volume	HSP
PCL	114	1.09	104.587156	17.2
PCLMA	114	1.09	104.587156	16.7
PCLMAA	114	1.09	104.587156	17.4
PLA	152	1.24	122.5806452	19.8
PLAMA	152	1.24	122.5806452	19.3
PLAMAA	152	1.22	124.5901639	19.7
PTMC	102	1.32	77.27272727	16.5
PTCMA	102	1.31	77.86259542	17.6
PTMCAA	102	1.3	78.46153846	20.8
PEGDA	170	1.08	157.4074074	18.5
NVP	111	1.04	106.7307692	20.8
trandolapril	450.537	1.1	409.5790909	20.5
pitavastatin	421.461	1.2	351.2175	23.3

Table S2. Calculated Flory-Huggins interaction parameter (χ) for the different materials combinations

Flory-Huggins interactions parameter		
	PEGDA	NVP
PCL	0.071	0.047
PCLMA	0.137	0.061
PCLMAA	0.051	0.042
PLA	0.084	0.003
PLAMA	0.032	0.006
PLAMAA	0.072	0.003
PTMC	0.125	0.075
PTCMA	0.025	0.041
PTMCAA	0.167	0.000
PEGDA	0.000	0.004

Table S3. Viscosity measurements

	oligomer	solvent	Viscosity (mPa·s)							
			70°C		60°C		50°C		40°C	
			Mean	SD	Mean	SD	Mean	SD	Mean	SD
1	PCL	PEGDA	25.83	0.60	36.45	3.26	38.45	2.54	51.21	0.45
2	PCLMA	PEGDA	16.33	1.24	23.73	2.42	26.27	2.42	38.44	0.54
3	PCLMAA	PEGDA	47.51	0.86	68.51	1.67	82.19	4.64	103.40	2.65
4	PCL	NVP	10.62	0.79	14.32	1.70	15.18	1.59	21.18	0.93
5	PCLMA	NVP	4.03	0.11	6.40	0.48	7.86	1.06	10.46	0.31
6	PCLMAA	NVP	14.50	1.55	31.41	2.34	47.83	3.96	106.00	10.89
7	PLA	PEGDA	13.74	0.32	23.94	0.97	28.32	0.89	46.42	2.48
8	PLAMA	PEGDA	22.49	1.60	34.94	2.51	40.55	2.97	68.20	3.48
9	PLAMAA	PEGDA	31.10	1.25	48.85	1.78	56.05	1.29	x	x
10	PLA	NVP	4.44	0.32	6.91	0.81	7.63	1.65	11.00	1.27
11	PLAMA	NVP	6.04	0.23	9.16	0.47	10.30	0.46	15.17	0.27
12	PLAMAA	NVP	10.81	0.82	18.57	1.01	21.66	1.01	34.45	0.62
13	TMC	PEGDA	5.86	0.16	9.75	0.54	10.82	0.58	16.67	0.38
14	TMCMA	PEGDA	12.67	0.10	19.69	0.71	22.18	0.48	34.77	0.81
15	TMCMAA	PEGDA	15.06	0.46	24.71	0.69	28.02	0.33	44.40	1.81
16	TMC	NVP	1.51	0.24	3.16	0.41	4.13	0.65	5.89	0.75
17	TMCMA	NVP	5.44	0.35	8.00	0.22	8.36	0.35	11.62	0.11
18	TMCMAA	NVP	8.61	0.27	12.96	0.10	13.63	0.42	19.38	1.18

Table S4. Surface tension measurements

	oligomer	solvent	Surface Tension (mN·m)	
			Mean	SD
1	PCL	PEGDA	38.31	0.48
2	PCLMA	PEGDA	38.25	0.50
3	PCLMAA	PEGDA	37.90	0.26
4	PCL	NVP	39.57	0.55
5	PCLMA	NVP	39.03	0.69
6	PCLMAA	NVP	39.02	0.52
7	PLA	PEGDA	37.60	0.76
8	PLAMA	PEGDA	37.85	0.67
9	PLAMAA	PEGDA	38.18	0.46
10	PLA	NVP	38.68	0.64
11	PLAMA	NVP	38.67	0.42
12	PLAMAA	NVP	34.33	4.32
13	TMC	PEGDA	38.67	0.63
14	TMCMA	PEGDA	38.02	0.75
15	TMCMAA	PEGDA	37.85	0.90
16	TMC	NVP	40.00	0.66
17	TMCMA	NVP	39.35	0.65
18	TMCMAA	NVP	39.43	0.86

Table S5. Printability screening. Z parameter. Reis & Derby used numerical simulation of drop formation to propose $10 > Z > 1$ for stable drop formation.

	oligomer	solvent	Z Parameter			
			70°C	60°C	50°C	40°C
1	PCL	PEGDA	1.14	0.81	0.77	0.57
2	PCLMA	PEGDA	1.80	1.24	1.12	0.76
3	PCLMAA	PEGDA	0.62	0.43	0.36	0.28
4	PCL	NVP	2.78	2.06	1.94	1.39
5	PCLMA	NVP	7.27	4.58	3.73	2.80
6	PCLMAA	NVP	0.00	0.00	0.00	0.00
7	PLA	PEGDA	2.17	1.24	1.05	0.64
8	PLAMA	PEGDA	1.33	0.86	0.74	0.44
9	PLAMAA	PEGDA	0.97	0.61	0.54	x
10	PLA	NVP	6.71	4.32	3.91	2.71
11	PLAMA	NVP	4.94	3.26	2.90	1.97
12	PLAMAA	NVP	2.60	1.51	1.30	0.82
13	TMC	PEGDA	5.11	3.07	2.77	1.80
14	TMCMA	PEGDA	2.34	1.51	1.34	0.85
15	TMCMAA	PEGDA	1.97	1.20	1.06	0.67
16	TMC	NVP	19.87	9.46	7.25	5.09
17	TMCMA	NVP	5.46	3.71	3.55	2.55
18	TMCMAA	NVP	3.45	2.29	2.18	1.53

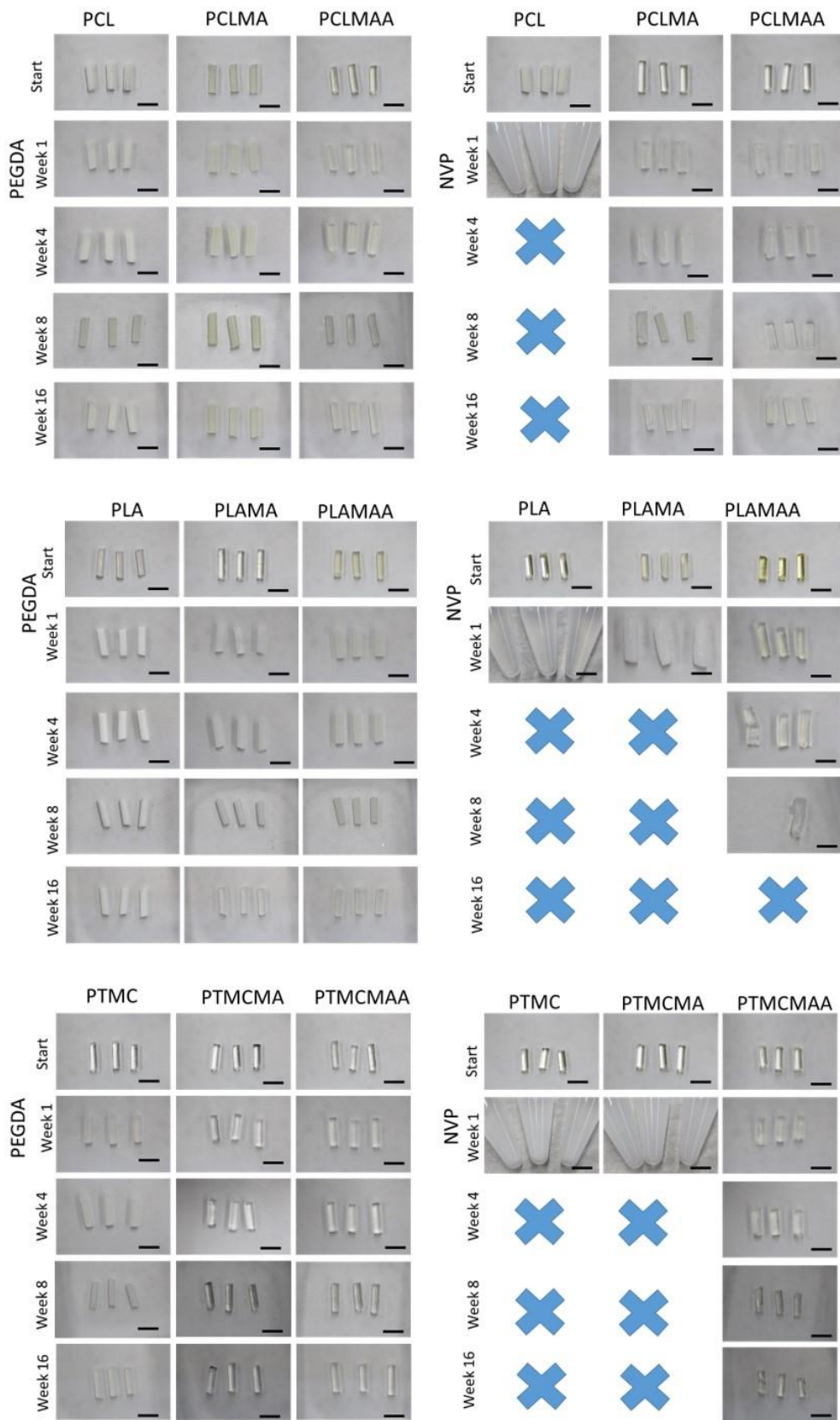
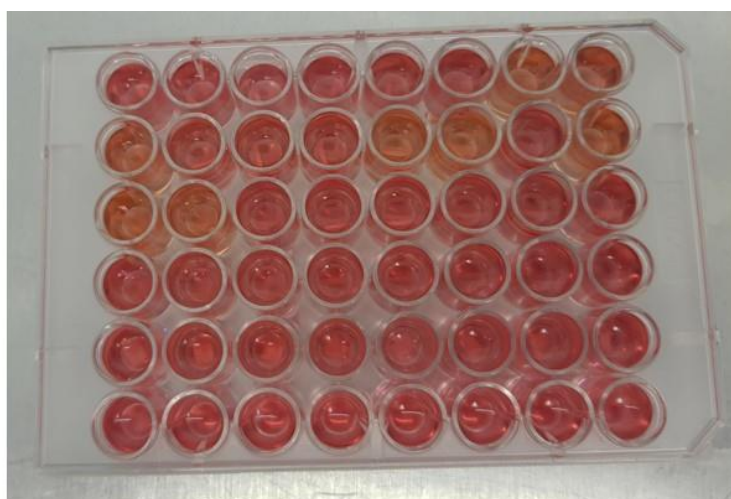


Figure S5. Images of casted samples during the in vitro degradation studies. Scale bars represent 4 mm.



PCL	PCL	PCL	PCLMA	PCLMA	PCLMA	PCLMAA	PCLMAA
PCLMAA	PLA	PLA	PLA	PLAMA	PLAMA	PLAMA	PLAMA
PLAMAA	PLAMAA	TMC	TMC	TMC	TMCMA	TMCMA	TMCMA
TMCMAA	TMCMAA	TMCMAA	CONTROL	CONTROL	CONTROL	CONTROL	CONTROL
CONTROL							
CONTROL							

Figure S6. We saw no significant reduction in cell viability on day 3 when compared to the control group (cells cultured in standard medium). However, there was a 10% viability reduction on day 30 when the cells were cultured with medium from the PLA based samples (**Figure 2B**), most likely due to the acidic degradation by products.^[18] This images shows pH changed observed in the medium after been incubated with the samples for 30 days. The change in pH was detected due to the presence of phenol red in medium. The lighter the colour the more acidic the medium.

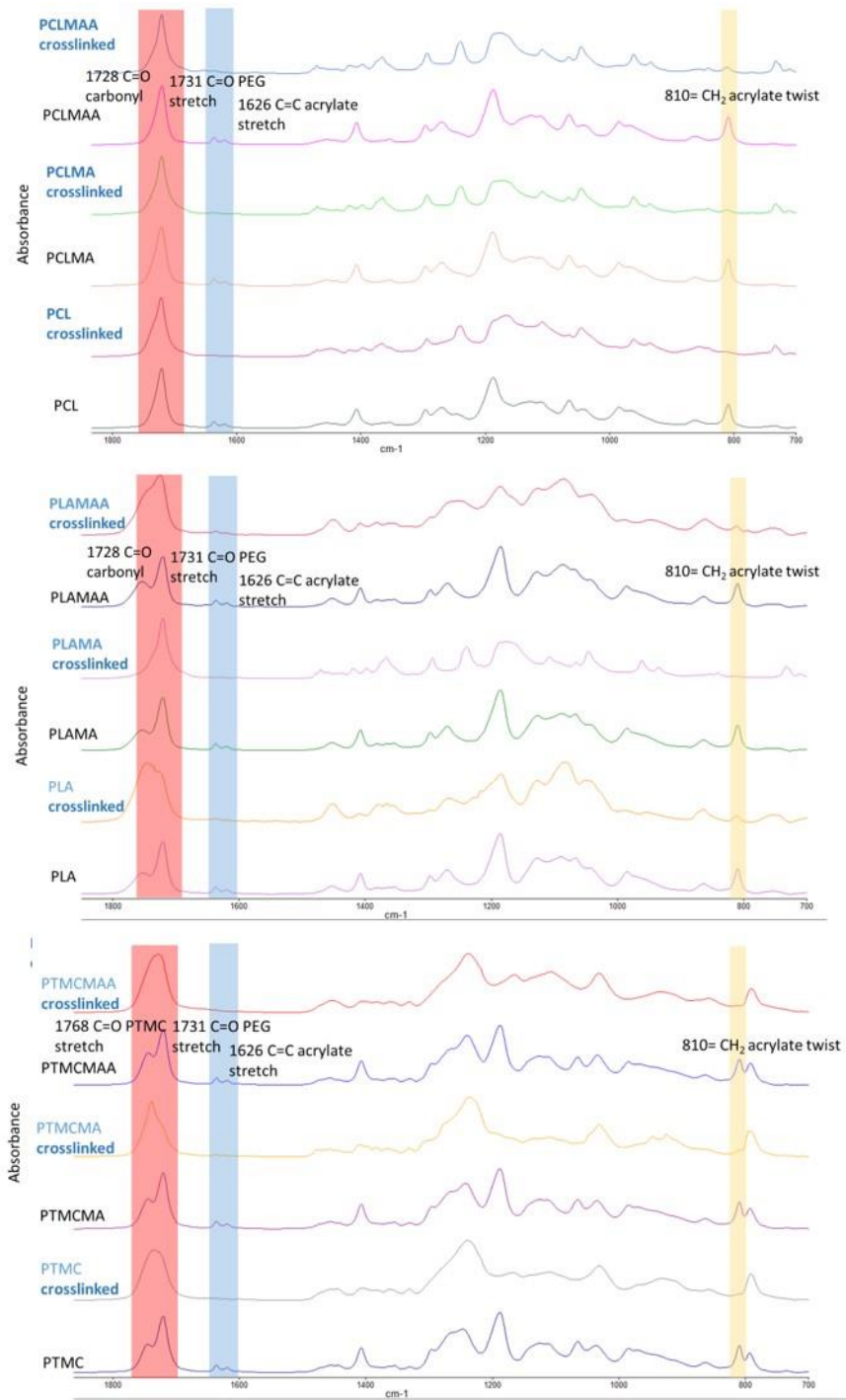


Figure S7. FTIR Evaluation of the degree of conversion of the casted samples.

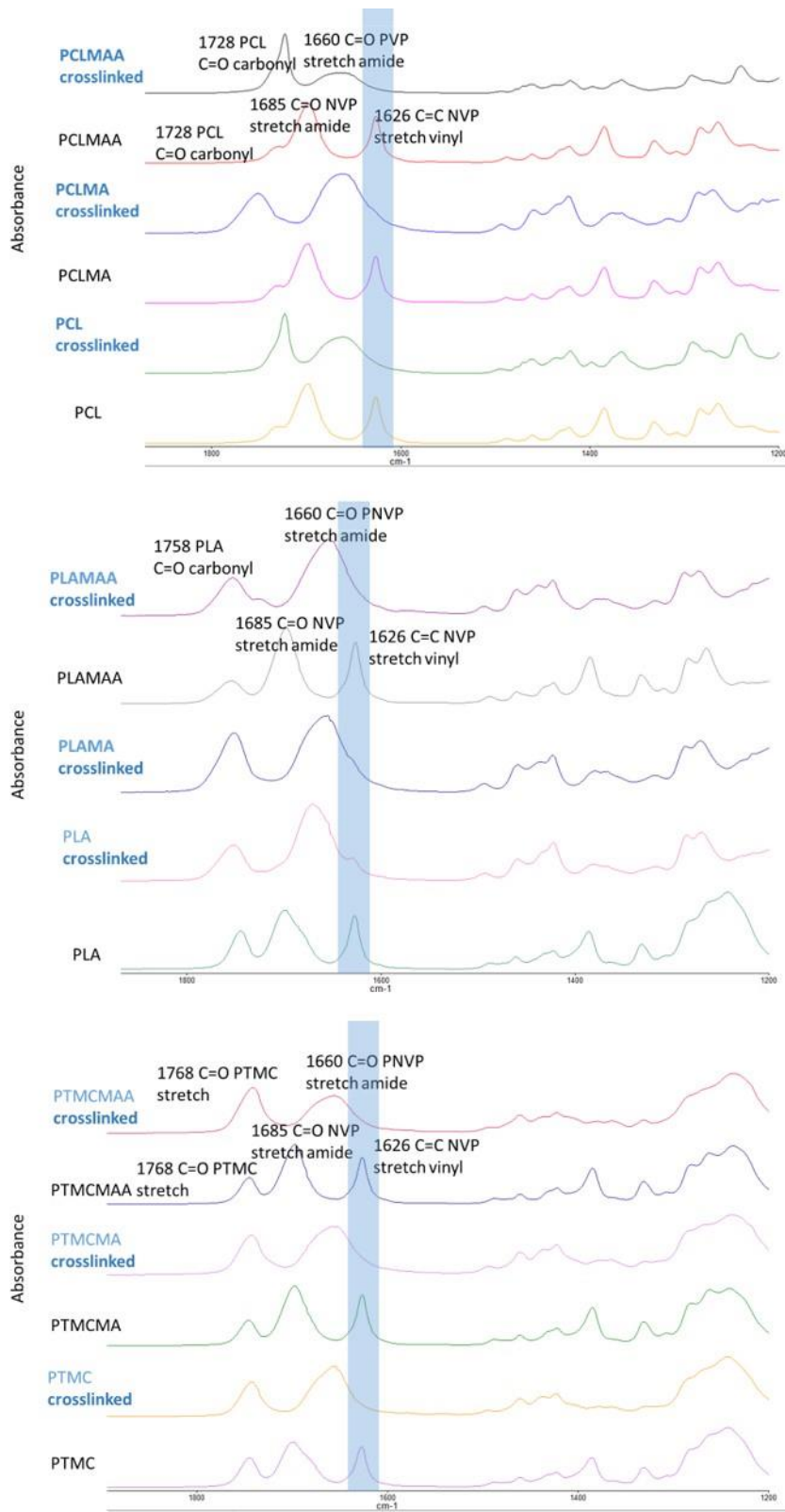
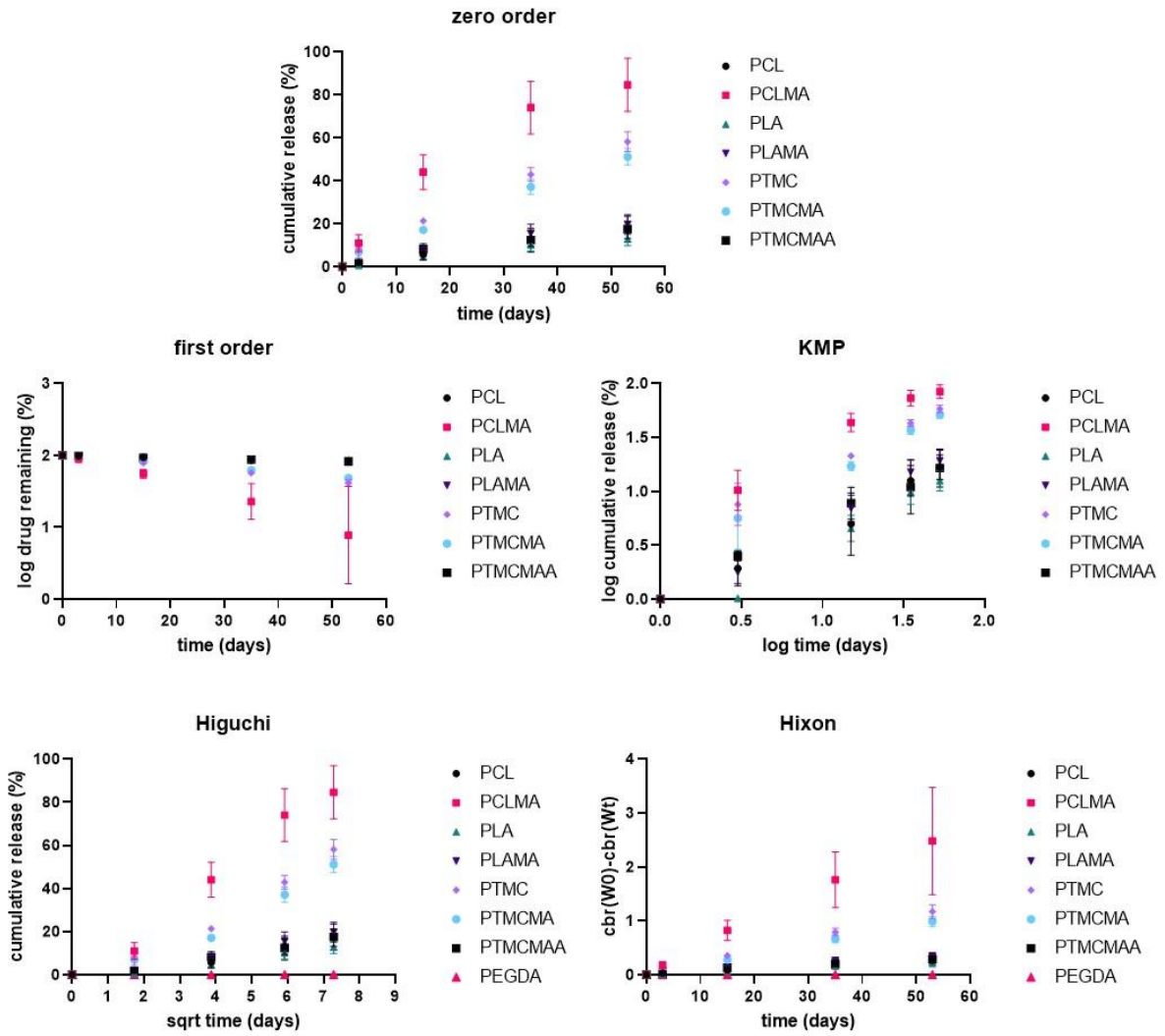


Figure S8. FTIR Evaluation of the degree of conversion of the casted samples.

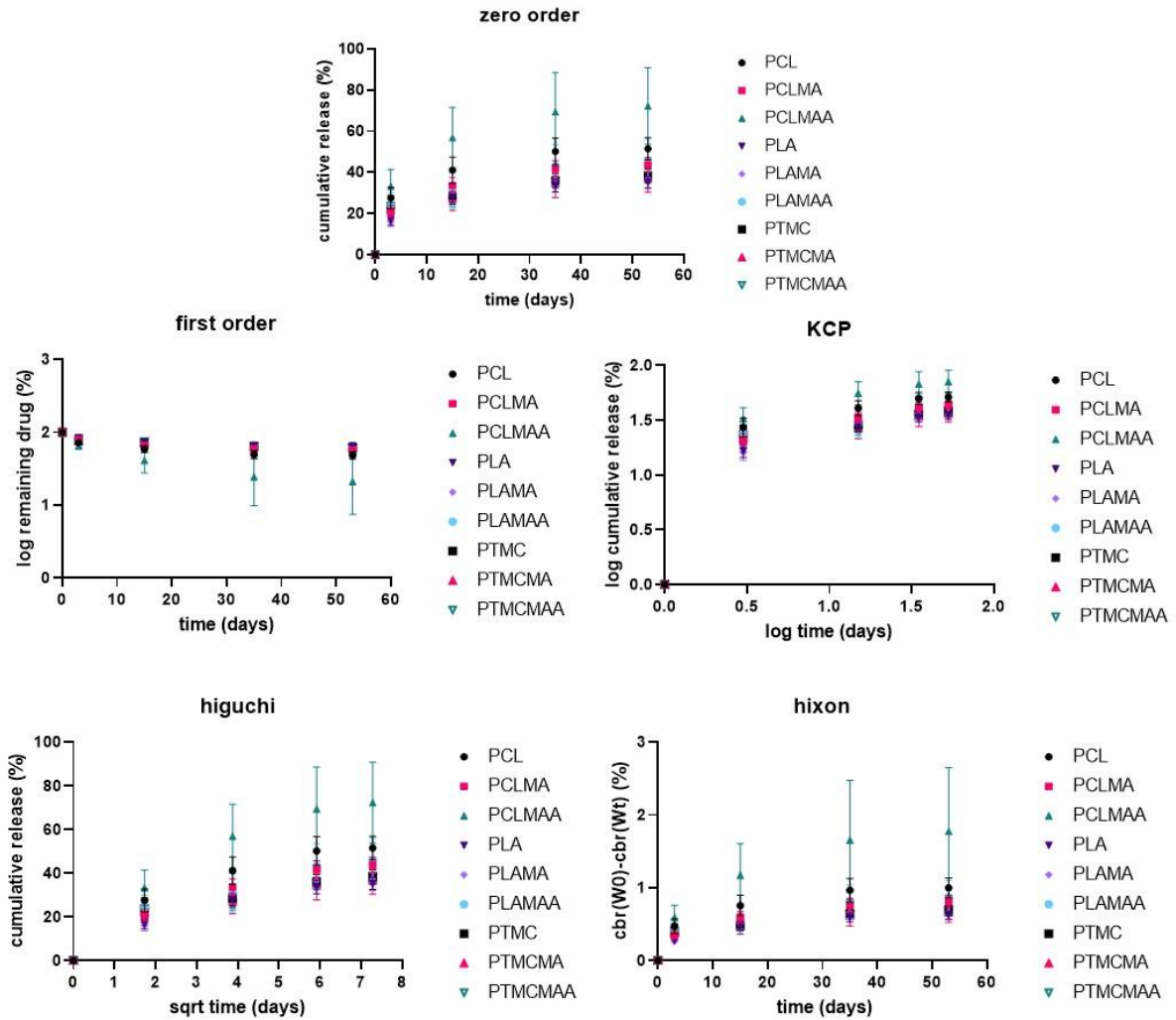
Table S6. Flory-Huggins interaction parameter of the different components of the formulations with trandolapril and pitavastatin.

χ	trandolapril	χ	pitavastatin
PCL	6.148	PCL	5.272
PCLMA	7.197	PCLMA	6.172
PCLMAA	5.752	PCLMAA	4.932
PLA	2.024	PLA	1.736
PLAMA	2.644	PLAMA	2.267
PLAMAA	2.141	PLAMAA	1.836
PTMC	7.640	PTMC	6.552
PTCMA	5.368	PTCMA	4.603
PTMCMAA	1.033	PTMCMAA	0.886
PEGDA	3.807	PEGDA	3.264
NVP	1.033	NVP	0.886



	PCL	PLCLMA	PLA	PLAMA	PTMC	PTMCMA	PTMCMAA
zero order	0.9895	0.9324	0.9817	0.9817	0.9888	0.9923	0.9686
first order	0.9929	0.9926	0.9853	0.9873	0.9974	0.9967	0.9769
KMP	0.9866	0.9342	0.9472	0.9935	0.9525	0.9744	0.992
Higuchi	0.9617	0.9853	0.9594	0.9594	0.9717	0.9614	0.9773
Hixon	0.9918	0.9966	0.9842	0.9856	0.9975	0.9971	0.9743

Figure S9. Cumulative release of trandolapril from the casted samples. Fitting of the release to different models. The R2 values are shown in the table.



	PCL	PCLMA	PCLMAA	PLA	PLAMA	PLAMAA	PTMC	PTMCMA	PTMCMAA
zero order	0.6749	0.7196	0.7182	0.7094	0.7314	0.7347	0.6417	0.6527	0.7734
first order	0.7553	0.7824	0.8959	0.7559	0.7768	0.8121	0.7022	0.7141	0.8299
KMP	0.7139	0.7424	0.7297	0.7536	0.774	0.7186	0.6888	0.6929	0.7481
Higuchi	0.885	0.9157	0.9163	0.9102	0.9247	0.9106	0.8462	0.8541	0.9371
Hixon	0.729	0.762	0.8368	0.7407	0.762	0.7871	0.682	0.6936	0.8117

Figure S10. Cumulative release of trandolapril from the casted samples. Fitting of the release to different models. The R² values are shown in the table. When the formulations contained PEGDA/NVP (1:1) as the reactive solvent, there was an initial burst release of more than 20% in all cases, directly attributable to the dissolution of PVP when immersed in an aqueous environment.

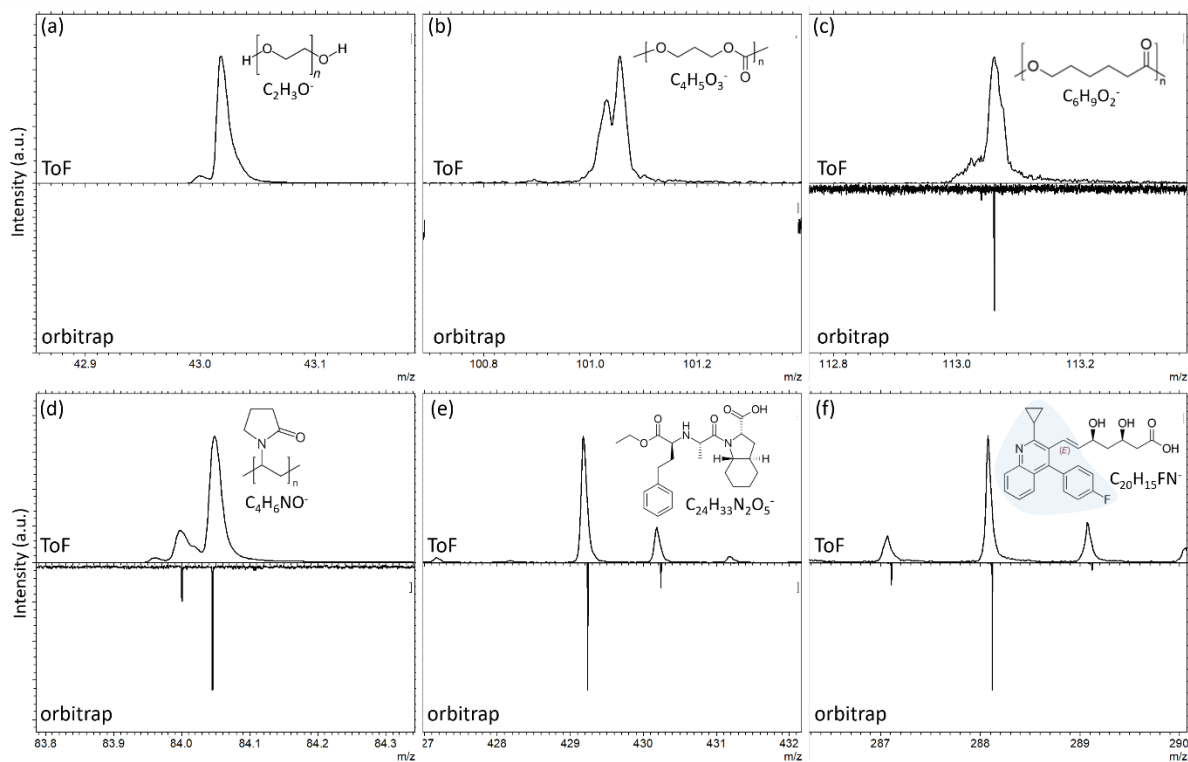


Figure S11. Zoomed in view of ToF-SIMS (top half of each item) and orbiSIMS (bottom half of each item) spectra showing peaks of characteristic secondary ions for each of the main compounds in the printed samples. (a) PEGDA ($C_2H_3O^-$). (b) PCLDA ($C_4H_5O_3^-$). (c) PTMCA ($C_6H_9O_2^-$). (d) PVP ($C_4H_6NO^-$). (e) Trandolapril ($C_{24}H_{33}N_2O_5^-$) (f) Pitavastatin ($C_{20}H_{15}FN^-$).

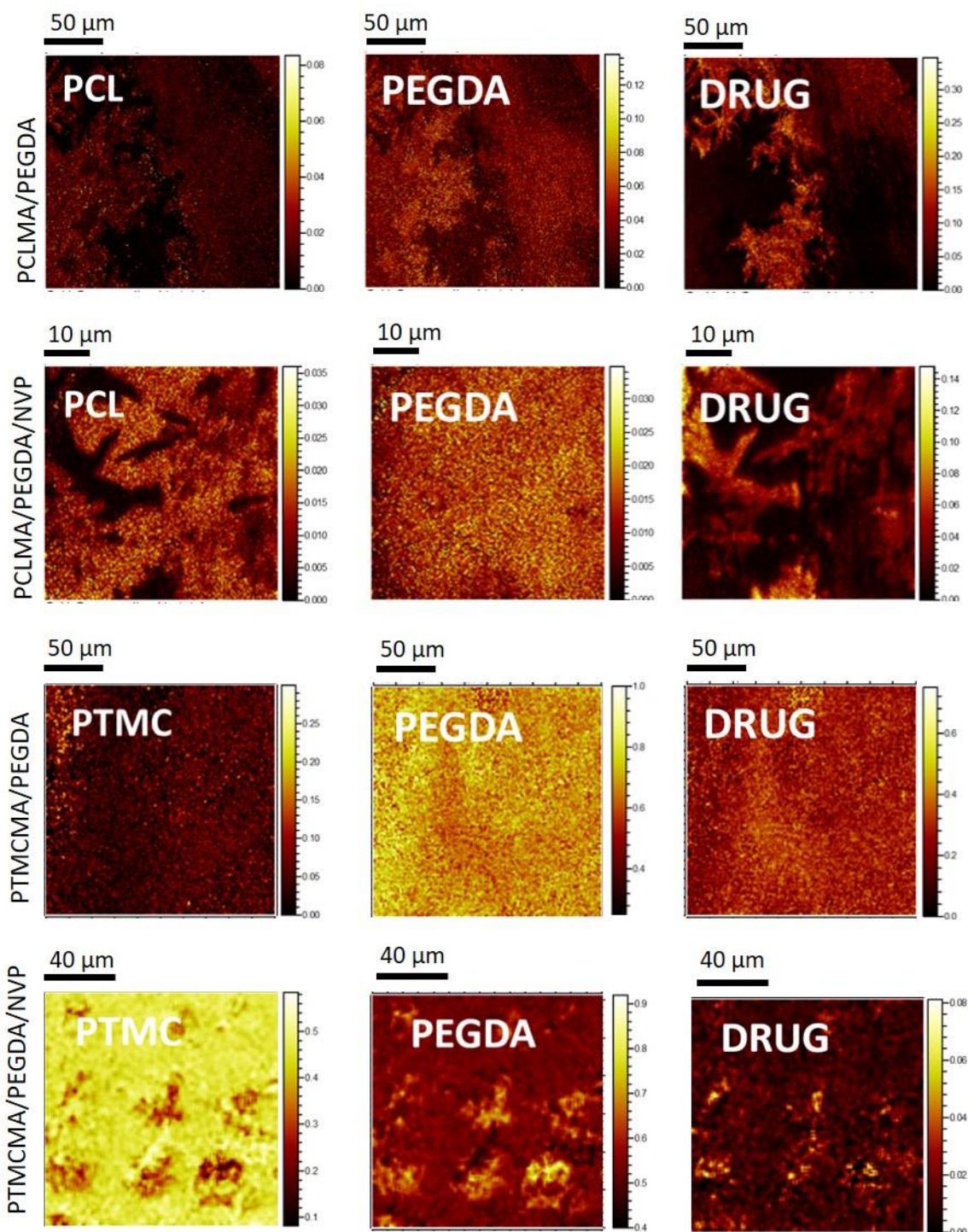


Figure S12. ToF SIMS of the printed samples. Ion images represent PCL ($C_4H_5O_3^-$), PTMC ($C_4H_5O_3^-$), PEGDA ($C_2H_3O^-$), trandolapril ($C_{24}H_{33}N_2O_5^-$) and pitavastatin ($C_{20}H_{15}FN^-$)

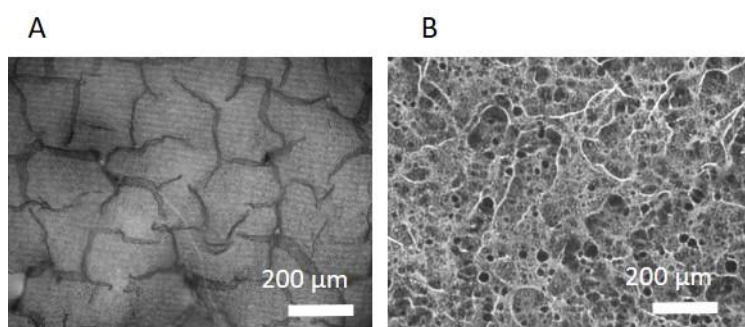


Figure S13. (A) Microscopy images of PTMCMA/PEGDA/PVP and (B) PLAMA/PEGDA/PVP after 24 hours immersed in PBS at 37 C.

References

- [1] L. Ruiz-Cantu, A. Pearce, L. Burroughs, T. Bennet, C. Vasey, R. Wildman, D. Irvine, C. Alexander, V. Taresco, *Macromol. Chem. Phys.* **2018**, *220*, 1800459.
- [2] K. Fukushima, *Polym. J.* **2016**, *4880*, 1103.
- [3] H. Qian, A. R. Wohl, J. T. Crow, C. W. MacOsco, T. R. Hoye, *Macromolecules* **2011**, *44*, 7132.
- [4] V. Taresco, J. Suksiriworapong, I. D. Styliari, R. H. Argent, S. M. E. Swainson, J. Booth, E. Turpin, C. A. Laughton, J. C. Burley, C. Alexander, M. C. Garnett, *RSC Adv.* **2016**, *6*, 109401.
- [5] D. Li, Y. Jiang, S. Lv, X. Liu, J. Gu, Q. Chen, Y. Zhang, *PLoS One* **2018**, *13*, e0193520.
- [6] M. Teodorescu, M. Bercea, *Polym. - Plast. Technol. Eng.* **2015**, *54*, 923.
- [7] H. Foltmann, A. Quadir, *Drug del Tech.* **2008**, *8*, 22.
- [8] T. J. White, W. B. Liechty, C. A. Guymon, *J. Polym. Sci. Part A Polym. Chem.* **2007**, *49*, 4062.
- [9] C. M. A. Lopes, M. I. Felisberti, *Biomaterials* **2003**, *24*, 1279.
- [10] C. F. Brunius, U. Edlund, A. C. Albertsson, *J. Polym. Sci. Part A Polym. Chem.* **2002**, *40*, 3652.
- [11] L. Xue, J. Zhang, Y. Han, *Prog. Polym. Sci.* **2012**, *37*, 564.
- [12] B. Imre, K. Renner, B. Pukánszky, *Express Polym. Lett.* **2014**, *8*, 2.
- [13] Z. Zhou, L. Ruiz Cantu, X. Chen, M. R. Alexander, C. J. Roberts, R. Hague, C. Tuck, D. Irvine, R. Wildman, *Addit. Manuf.* **2019**, *29*, 100792.

- [14] J. E. Fromm, *IBM J. Res. Dev.* **1984**, 28, 322.
- [15] N. Reis, B. Derby, *MRS Proc.* **2000**, 625, 117.
- [16] G. F. Trindade, M. L. Abel, J. F. Watts, *Chemom. Intell. Lab. Syst.* **2018**, 182, 180.
- [17] M. K. Passarelli, A. Pirkl, R. Moellers, D. Grinfeld, F. Kollmer, R. Havelund, C. F. Newman, P. S. Marshall, H. Arlinghaus, M. R. Alexander, A. West, S. Horning, E. Niehuis, A. Makarov, C. T. Dollery, I. S. Gilmore, *Nat. Methods* **2017**, 14, 1175.
- [18] M. S. Taylor, A. U. Daniels, K. P. Andriano, J. Heller, *J. Appl. Biomater.* **1994**, 5, 151.